INVESTIGATION OF SURFACE ROUGHNESS EFFECT ON THE FLOW STRUCTURE AROUND A SPHERE

Conference Paper · September 2011

CITATION
1

READS
957

5 authors, including:

Muammer Ozgoren
Selcuk University
59 PUBLICATIONS **697** CITATIONS
SEE PROFILE

Sercan Dogan
Konya Technical University
26 PUBLICATIONS **95** CITATIONS
SEE PROFILE

Abdulkerim Okbaz
Dogus Universitesi
36 PUBLICATIONS **104** CITATIONS
SEE PROFILE

Besir Sahin
Cukurova University
166 PUBLICATIONS **2,231** CITATIONS
SEE PROFILE

6. ANKARA INTERNATIONAL AEROSPACE CONFERENCE
14-16 September 2011 - METU, Ankara TURKEY

AIAC-2011-077

INVESTIGATION OF SURFACE ROUGHNESS EFFECT ON THE FLOW STRUCTURE AROUND A SPHERE

Muammer Ozgoren[1]
Sercan Dogan[2]
Abdulkerim Okbaz[3]
Selcuk University
Konya, Turkey

Besir Sahin[4]
Huseyin Akilli[5]
Cukurova University
Adana, Turkey

ABSTRACT

This paper presents the experimental investigation of turbulent structures of flow around a smooth and roughened sphere. Dye visualization and particle image velocimetry (PIV) techniques were performed to examine surface roughness effects on the wake for Reynolds numbers between 2,500 and 10,000. Experiments were carried out in open water channel in which Reynolds number is restricted in the laminar flow region based on the sphere diameter with a 42.5mm due to the experimental facility conditions. In order to control passively flow structure, sphere surface is roughened in terms of circular holes having a 3mm diameter and 2mm depth to induce a turbulent boundary layer on the sphere surface because turbulent boundary layer flow has a larger momentum than laminar boundary layer flow and thus delays separation. In order to demonstrate the roughness effects, flow characteristics such as instantaneous velocity vectors, vorticity contours, time-averaged streamline patterns, Reynolds stress correlations and streamwise and cross-stream velocity fluctuations for both the smooth and roughened sphere were compared. Dye visualization showed that the presence of the roughness on the sphere surface caused the dye filaments to become shortened and smoothed for Re=2500 and induce earlier forming of Kelvin Helmholtz vortices for Re=2500 and Re=5000. The roughened surface causes local flow separation and triggers the shear layer instability along the separating shear layer, resulting in the generation of large turbulence intensity on the sphere surface and hence the flow reattaches to the sphere surface with a high momentum near the wall and overcomes a strong adverse pressure gradient formed in the rear sphere surface. It is observed from the time-averaged streamline patterns that the roughness retards the flow separation from the sphere while the saddle point becomes closer the sphere for increasing Reynolds number. The reverse flow region in the wake is significantly reduced and the motion in that region also becomes weak owing to the roughened surface.

Keywords: Flow visualization; Instability; Passive control; PIV; Roughness; Sphere; Wake flow; Vorticity; Vortex shedding

INTRODUCTION

The flow around bluff bodies is of great interest for a large number of engineering applications such as pneumatic conveying, combustion, conveying of sediment materials in the river and conduit, sport balls, manned/unmanned submarine research vehicles, flow-structure interaction in aerodynamics and hydrodynamics. The flow fields encountered in many engineering applications are around a sphere, and are highly three-dimensional, unsteady, separated and turbulent.

[1] Assoc.Prof.Dr, Mechanical Engineering Department, email: mozgoren@ selcuk.edu.tr
[2] Research Assistant, Mechanical Engineering Department, Email: sercandogan@ selcuk.edu.tr
[3] Project Assistant, Mechanical Engineering Department, Email: abdulkerimokbaz87@ gmail.com
[4] Prof.Dr, Mechanical Engineering Department, Email: bsahin@cu.edu.tr
[5] Assoc.Prof.Dr, Mechanical Engineering Department, Email: hakilli@cu.edu.tr

Gad-el-hak [17] pointed out that the ability to manipulate a flow field to effect a desired change is of immense practical importance. As a scientific discipline and as a technological curiosity, flow control is perhaps more hotly pursued by scientists and engineers than any other area in fluid mechanics. Flow control involves passive or active devices to effect a beneficial change in wall bounded or free-shear flows. Whether the task is to delay/advance transition, to suppress/enhance turbulence or to prevent/provoke separation, useful end results include drag reduction, lift enhancement, mixing augmentation, heat transfer enhancement and flow-induced noise suppression. Passive control is applied by means of fixed or static devices such as roughness, splitter plate, trip wire, natural ventilation, streamlining the bluff body, helical strakes, perforated surface, ribbons, hemi spherical surface control bumps, spoiler adding and so on that modify the flow while active control is realized by dynamic actuators such as MEMS, small means of jets, acoustic transducers, suction etc. and requires some (ideally small) energy input.

Active and passive flow control methods of boundary layer and wake region have been studied for decades. However, there have specially been only a few studies of flow structure and its control methods in the downstream of a sphere using the particle image velocimetry (PIV) technique. When a bluff body is subjected to a fluid flow at sufficiently large Reynolds numbers, the flow separates from a wider section of the body giving rise to periodic vortex shedding from either sides of the body. This alternate vortex shedding characterized by definite periodicity would cause fluctuating pressure forces on the surfaces of the body. The size of the separation region depends on Reynolds number, roughness and turbulence intensity. The drag reduction and turbulence intensity diminishing can be performed by using roughness on the body. In the present study, for passive control purpose in the wake region of the sphere, the sphere having a circular roughness formation over the entire sphere that is very similar to the dimples on the golf ball surface is used. Some of the studies about the smooth and modified sphere surface are summarized as follows. Although several studies have been experimentally and numerically conducted for understanding the characteristics of flow over a sphere, there have been only a few works on control of flow over a sphere using passive and active devices (Achenbach [30]; Bearman & Harvey [28]; Kim & Durbin [24]; Suryanarayana & Meier [18]; Suryanarayana & Prabhu 2000). As for passive devices, Achenbach [30] and Bearman & Harvey [28] applied surface roughness and dimples on the sphere, respectively. Both studies achieved maximum drag reduction of nearly 50% in the sub-critical region, but the drag-reduction patterns by dimples was essentially different from that by surface roughness.

A different approach of controlling flow over a sphere was taken by Kim & Durbin [24]. Noting that there are two distinct frequencies existing in the shear layer and wake, they applied an acoustic forcing at a wide range of frequencies from the wake instability frequency to the shear-layer-instability frequency to flow over a sphere at much lower Reynolds numbers (Re ≤10,000) than those investigated using the passive control devices. They showed that the drag is increased significantly by the forcing and the size of the recirculation region is reduced with stronger motion inside, and they concluded that triggering the shear-layer instability or wake instability does not produce any drag reduction.

Kiya et al. [13] and Sakamoto and Haniu [22] classified sphere wake patterns according to Strouhal number in the Reynolds number from Re = 300 to 40,000. They observed vortex-tube pulsations and periodic vortex shedding incorporating asymmetric flow, as well as an irregularly rotating separation angle, a cylindrical-shaped shear layer instability, and irregular shedding with wavy progress of the wake. Kim and Durbin [24] found two frequency modes in the turbulent wake downstream of a sphere, which are related to the small-scale instability of the separating shear layers and to the large scale instability of the wake. Werle [26] visualized sphere wake in a water tunnel using dye at $Re = 1.6x10^4$ to see the recirculating flow downstream of a sphere and the shear layer instability of a ring-shaped vortex. At the first time, Achenbach [30, 31] visualized the vortical structure of sphere wake at Re = 1000 using a dye method and measured skin friction to investigate flow-separation angles in the range of $Re = 10^5–10^6$. The experiments of Taneda [22] show that in the range $3.8x10^5 < Re < 1.0x10^6$ the sphere wake forms a pair of streamwise line vortices at a short distance from the streamwise axis and the vortex pair rotates slowly and randomly about that axis. A nearly constant drag coefficient over a certain Reynolds number range was also found in the other types of surface modifications on a sphere. For example, Maxworthy [32] obtained this behavior of drag coefficient by placing a trip wire at a front-surface location. Nakamura and Tomonari [25] observed the same behavior by attaching a narrow roughness strip at a front-surface position. However, there was no discussion on the reason why the reduced drag coefficient remains nearly constant with these surface modifications.

Jeon et al. [10] performed an active control of flow over a sphere for drag reduction using a time-periodic blowing and suction at a sub-critical Reynolds number of Re =10^5. The forcing-frequency range considered was one to thirty times the natural vortex-shedding frequency. With the periodic blowing and suction, the drag on the sphere decreased by nearly 50% for forcing frequencies larger than a critical frequency. For forcing frequencies smaller than this critical frequency, drag was either nearly the same as, or slightly smaller than, that without forcing. The disturbances from the high-frequency forcing grow inside the boundary layer and delay the first separation while maintaining laminar separation, and they grow further along the separated shear layer and high momentum in the free stream is entrained toward the sphere surface, resulting in the reattachment of the flow (thus forming a separation bubble above the sphere surface) and the delay of the main separation.

Alamnar [11] used Spalart and Allmaras turbulence model to simulate turbulent flow around a 43mm diameter smooth sphere with 245 suction and blowing holes and a golf ball with 245 dimples. The holes and dimples were 0.3 and 3.7-mm in diameter, respectively. The simulation revealed stable vortical flow structure inside the dimples. The predicted drag coefficient for the golf ball was 52 % lower than that of the sphere, which was 0.23. The simulation was carried out at Re=2x10^5,corresponding to Ma=0.2.

Bakic [12] presented that the results of LDA measurements for three different experimental configurations (flow around a smooth sphere, flow around a sphere with trip-wire and flow around a sphere in a flow with high free-stream turbulence). Experiments were carried out in a wind tunnel at same Reynolds number Re=51,500, except in the case of a sphere in a flow with high free-stream turbulence where the Reynolds number was R=48,000. The flow and turbulence characteristics in the these three cases were substantially different. Results for the sphere with trip-wire showed that the separation point moves downstream due to the transition of the boundary layer at the sphere surface. The lowest Reynolds stresses result found for the sphere with a trip-wire.

J. Choi et al. [8] stated that the best of the authors' knowledge, the only conjecture available in the literature was made by Bearman and Harvey [19, 28] who suggested that dimples generate discrete vortices energizing the boundary layer flow. J. Choi et al. [9] examined mechanism of drag reduction by dimples on a sphere such as golf-ball dimples by measuring the streamwise velocity above the dimpled surface to prove this conjecture. They stated that dimples cause local flow separation and trigger the shear layer instability along the separating shear layer, resulting in the generation of large turbulence intensity. They recorded that a very low drag coefficient of a dimpled sphere such as a golf ball results from the generation of separation bubbles inside dimples and the delay of separation. Their study suggests that generation of a separation bubble, i.e., a closed-loop streamline consisting of separation and reattachment, on a body surface is an important flow-control strategy for drag reduction on a bluff body through the shear layer instability.

Lee and Jang [6] reported only the vortical structures of sphere wake in the streamwise plane at Re = 11,000 by using a PIV technique to clarify recirculating vortices, recirculation length, and the spatial distributions of turbulence statistics. They expressed that their results could enhance understanding on the vortical flow structure and shear-layer instability inside the near-wake of a sphere and provide useful experimental data for validating numerical predictions.

Kumar et al. [5] published a review of the passive control of Vortex-Induced Vibrations (VIV) through various means particularly emphasizing some recent inventions patented. The review indicates that, in practical applications especially in marine engineering situations, passive control measures such as employing a streamline fairing or a helical strake, prolong the life of offshore structures by protecting them from vortex-induced vibrations. They stated that four classes of are commonly identified as vortex induced vibrations, galloping, flutter and buffeting.

Ozgoren et al. [7] reported useful information about flow structure around a single sphere body as preliminary study. Recently, Ozgoren et al. [4] have been studied experimentally flow structure of a sphere and cylinder for Re=5,000 in a uniform flow from the point of flow physics and vortex formation lengths of large-scale Karman Vortex Streets and Kelvin-Helmholtz vortices. It was demonstrated that flow patterns of the sphere becomes very complex in the wake region under the influence of interactions between the solid body and flow. Flow separation angle of the cylinder was less than that of the sphere. Time averaged flow patterns of both the cylinder and sphere were very similar to each

other. The vorticity distribution of the sphere wake showed more waviness in cross-sectional planes than that of the cylinder. Enhancement levels of Reynolds stress correlations associated with cross-stream velocity for both geometries were clarified. The time-averaged turbulent structures were consistent with the visualized flow showing the onset of shear layer instability.

Ozgoren, Dogan et al. [3] have investigated experimentally passive control of vortical flow structure around a sphere by an o-ring for Re=5,000. O-rings with 2mm and 3mm diameters were located at the front side of the sphere having 42.5 mm diameter at angles of 45°, 50°, 55° and 70° to see its suppression effect in terms of dye experiment. They found from dye visualization that the controlled flow structure results of the sphere with 2mm o-ring at 55° was the most effective. It was obtained from the comparison of the smooth sphere and sphere with o-ring that the maximum locations of Reynolds stress correlations, the rms velocities in x and y directions occurred closer to the sphere base for the sphere with o-ring case although their magnitudes did not change considerably. These findings may be interpreted that the drag coefficient of the sphere with o-ring can be lower than that of the smooth sphere owing to the suppression effect of the o-ring in the wake region.

Ozgoren, Okbaz et al. [2] have studied on the flow characteristics of a smooth sphere and a vent sphere located in a uniform flow for the Reynolds number range 2,500≤Re≤10,000 quantitatively using the particle image velocimetry technique and qualitatively with dye visualization. The flow phenomena in the downstream regions of the sphere increase the instability of the vortical flow structure significantly. It is pointed out that the modified flow structure of the near wake of the vented sphere may be characterized by a pair of counter-rotating ring vortices, which have the effect of aerodynamically streamlining the sphere.

In the present study, the effect of a roughened surface on the flow around a sphere is experimentally investigated at subcritical Reynolds numbers of Re=5,000, 7,500 and 10,000 based on the free-stream velocity U_∞ and sphere diameter D. Results are discussed in terms of instantaneous and time-averaged flow features focusing on the wake structure for the smooth and roughened sphere. In the present study, for the first time the instantaneous and time-averaged velocity around the roughened sphere are measured using PIV technique.

EXPERIMENTAL METHOD

Experiments were performed in a large-scale open water channel with a test section length of 8,000 mm and a width of 1,000 mm at the Department of Mechanical Engineering at Cukurova University, Turkey. To perform the present experimental study, the test section made from 15 mm thick transparent plexiglas sheet, which had a total height of 750 mm, was filled with water to a level of only 450 mm. Before reaching the test chamber, the water was pumped into a settling chamber and passed through a honeycomb section and a two-to-one channel contraction. An overview of experimental system of the sphere is shown in Fig. 1. Free stream turbulence intensity of the flow is less than 0.5% in the range of the present Reynolds numbers, $\mathrm{Re} = (U_\infty D)/\nu$, based on the sphere diameter (D). Here, ν and D are kinematics viscosity and diameter of the sphere (D), respectively. U_∞ is the free-stream velocity taken as 117.6 to 235 mm/s for 5,000≤Re≤10,000. The sphere with a diameter of 42.5 mm was made of plexiglas so that the laser light propagates easily from them. In addition, water cell segment of the sphere equator with a diameter of 38.5mm and a wall thickness of 2.0 mm was created. It was filled with distilled water and had a total height of 8 mm in order to reduce largely the laser light deflection on the sphere. The sphere surface was highly polished to avoid effects of surface roughness. The laser sheet was located at 225 mm above the bottom surface of the channel while the water height h_w was 450 mm in all cases. The Froude number based on the water depth h_w was $Fr = U_\infty / \sqrt{g h_w}$ =0.056, which was subcritical flow region owing to the less than 1.0. To support the sphere in the water channel, a circular bar with a 5 mm diameter was connected to the sphere from the top. Disturbance effect of the support bar on the laser sheet location of the measurement plane that was observed by dye injection was negligible in the consideration of support diameter with respect to the sphere diameter. The solid blockage ratio of the sphere including support was 1.3 %. The vented sphere made of solid plexiglas and did not permit to pass the laser light. For dye visualization, dye ports with 0.7mm diameter are located on the equator of the sphere at angle values with respect to the flow direction as 0°, 70°,90°, 110°, 180°, 290°, 270° and 250°.

Nd:YAG laser was used to generate a laser sheet that was perpendicular to the axis for the sphere the symmetry axis and camera (i.e. equator of the sphere) was passed through them. A CCD camera

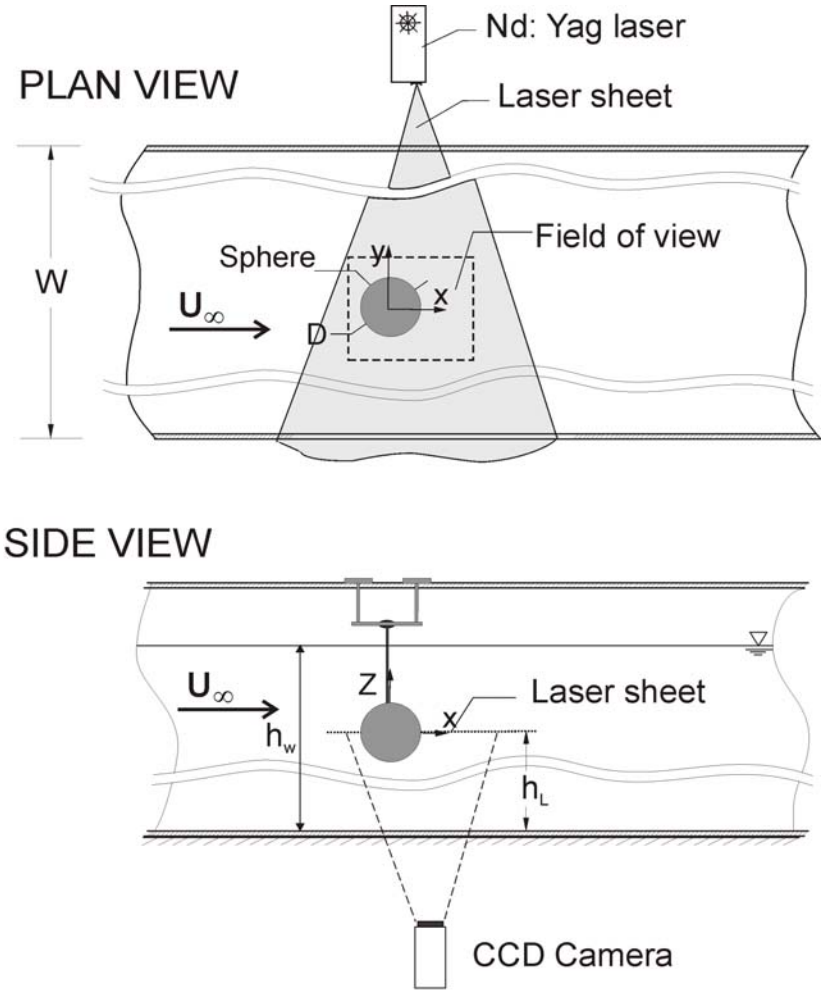

(a)

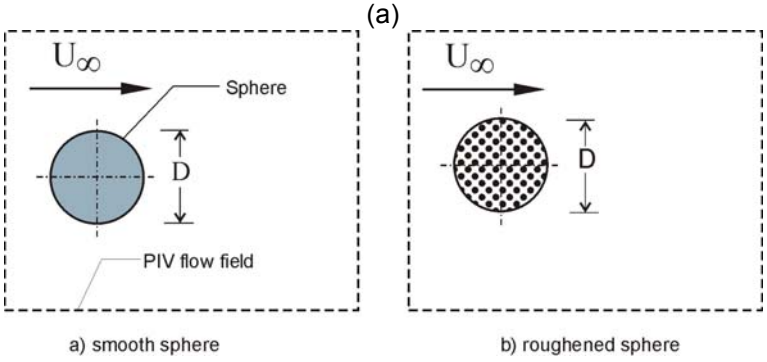

(b)

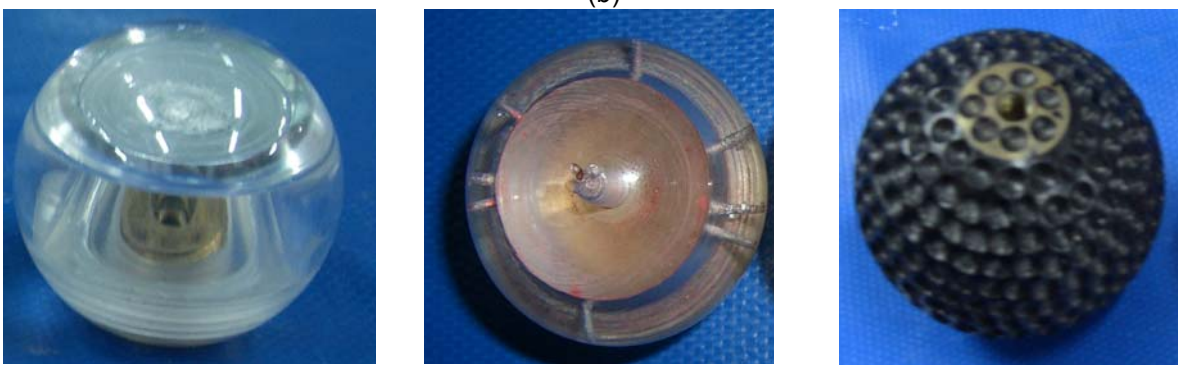

PIV Model | Dye Visualization Model | Roughened Model

(c)

Figure 1: Schematic view of (a) the experimental setup of PIV system, (b) sphere position for a smooth and a roughened sphere case and (c) photograph of the smooth and roughened sphere.

having a resolution of 1,600 x 1,186 pixels was used to record the images. The seeding particles with a diameter of 10 μm in the flow were silver metallic coated hollow plastic spheres. The densities of the particles and water are close enough so that the distribution of particles in suspension remains uniform for several hours. The high-image-density criterion was satisfied by ensuring that a minimum of approximately 20-30 particles was contained within the interrogation area. The illuminating laser sheet thickness in the flow field was approximately 1.5 mm. As shown in Fig. 1, the camera was mounted in a fixed position side of the water tank. Dantec Flow Grabber digital PIV software employing the cross-correlation algorithm was used to compute the raw displacement vector field from the particle image data. Roughness surface was formed by means of circular holes with 3 mm diameter and around 2 mm depth. The holes were approximately arranged as an equilateral triangle and total hole number is 410 as seen in Figure 1c.

An interrogation window of 32x32 pixels in the image was selected and converted to grid size approximately 1.44x1.44 mm^2 for the single sphere (0.034Dx0.034D). The overall fields of physical view were for both spheres, yielding to 7,227 (99x73) velocity vectors for whole taken images. During the interrogation process, an overlap of 50% was employed in order to satisfy the Nyquist criterion. Patterns of instantaneous particle images with a total of 350 images for a sequential series were taken at the rate of 15 Hz, thereby spanning 23.27 sec. Averaged patterns of the flow structure were calculated using the set of the instantaneous images. The laser sheet was generated from a dual pulsed Nd:YAG system, having the maximum output of 120 mJ per pulse, which had time delays of Δt =1.0-1.7 ms for the present experiments. Inappropriate displacement vectors caused by shadows, reflections, or laser sheet distortions in the flow field replaced by using bilinear interpolation between surrounding vectors in the post-processing step. This algorithm included magnification factor and image captured rate in order to calculate velocities from the valid vectors. The field was then smoothed by a Gaussian weighted averaging technique. To minimize distortion of the velocity field, a smoothing parameter of 1.3 was chosen. After having vector field, the vorticity patterns of the wake flow were determined from the velocity field using a finite difference scheme with an in-house software. The details of the effects of these factors can be found in the studies of Hart [15], Fouras and Soria [16], Westerweel [20], Adrian [21] and Keane and Adrian [23]. The factors contributing to uncertainty in the velocity measurement using the PIV technique were critically assessed, Westerweel [20] concluding that uncertainty estimation in the velocity measurement was less than 2%.

RESULTS AND DISCUSSION

Comparison of flow visualization of flow structure with laser illumination of Rhodamine dye injection technique around the smooth sphere (left column) and the roughened sphere (right column) for Re=2,500 and Re=5,000 is shown in Figures 2 and 3. The observed near-wake recirculating region is large and the wake performs a progressive wave motion. For the smooth sphere case, large coherent structures are clearly visible whereas the wake region shrinks into shorter size for the roughened sphere case. The evolution history of the shedding vortices designated with A, B, C, D and E shows the roll-up of the separated shear layer and pairing of vortices for the smooth sphere case. These vortices becomes weak and less concentrated for the roughened sphere case. Turbulence structure in the free shear layer is so chaotic that roll-up and pairing processes are clearly visible with a wavy form. Flow visualization shows that the far wake region continues to grow in size and produces a wave-like motion. At Re = 2,500, the separating shear layer persists downstream to form a cylindrical vortex sheet and its chaotic structure becomes manifest around two sphere diameter in the downstream direction as seen in the left column of Fig 2. It is clear that, for the case of the roughened sphere, the detaching shear layer is attracted to the sphere surface and the size of the recirculation region is reduced as compared to the cases of the smooth sphere in Fig. 2. Figure 3 shows these progresses of the vortices for Re=5,000. The shear layer formed after the separation of boundary layer is subject to Kelvin-Helmholtz instability, which causes the roll-up of small-scale vortex rings at nearly regular time intervals. As seen from over viewing all images in Figure 3, small-scale Kelvin-Helmholtz instability commence earlier for the roughened sphere case. It appears that for all cases with laminar boundary layer flow separation, the wake region flow structure is already turbulent and further downstream wave-like structure can be observed. A laminar flow separation was found to occur near the equator for the smooth sphere.

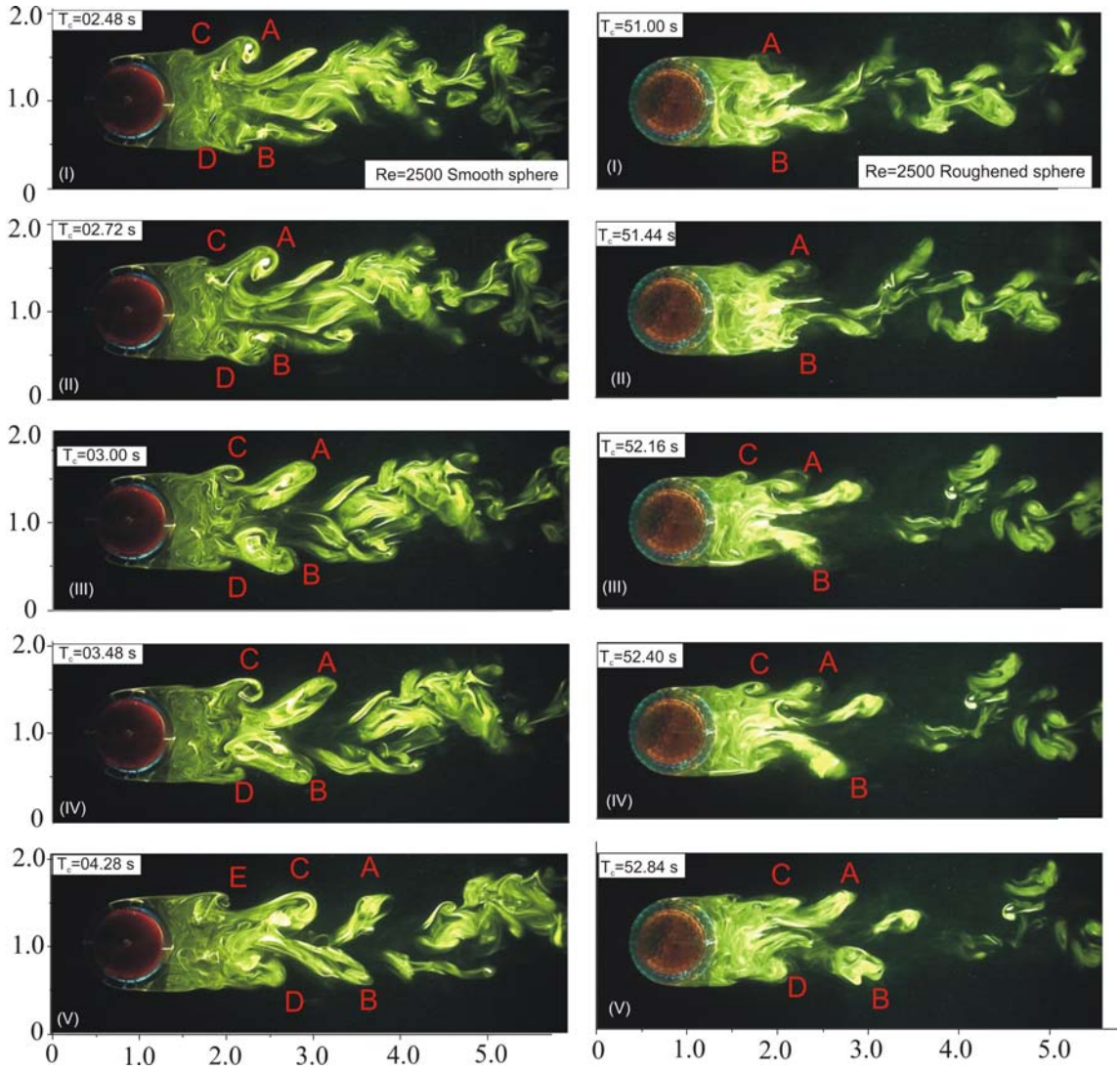

Figure 2: Comparison of flow visualization of flow structure with laser illumination of Rhodamine dye injection technique around the smooth sphere (left column) and the roughened sphere (right column) for Re=2,500.

The smooth laminar shear layers appeared to be axisymmetrically stable to the downstream location of about one sphere diameter. At Re=10,000, the vortex ring-shaped protrusions were observed with the onset of shear layer instability. Moreover, the transition from laminar to turbulence in the separated flow region occurred earlier at the higher Reynolds number of Re=10,000 than at Re=5,000. Roll-up and pairing of vortices in Figs 2 and 3 include the folding, rolling and breaking up a continuous vortex sheet into discrete vortices. Further downstream amalgamation of these vortices creates larger vortex structures. Successive amalgamation of pairs of neighboring vortices denoted by A to D in evident in the left column of Figs 2 and 3. During the pairing, vorticity is continuously being redistributed into larger eddies, whose wavelength and size increases at each interaction. Winant and Browand [29] have shown that merging of vortices was indeed the primary process governing the streamwise growth of the mixing layer thickness. The results of flow visualization indicated that the wake structure of a sphere and vortex configuration is more complicated for both of the sphere cases. Shedding small scale and larger scale vortices are the source of the different frequencies, which can give natural and sub-harmonic frequencies as recorded by Kim & Durbin [24] and Bakic [12].

Comparisons of instantaneous velocity fields V and instantaneous vorticity contours ω^* around the smooth sphere (left column) and roughened sphere (right column) for $5{,}000 \leq Re \leq 10{,}000$ are respectively displayed in Figs 4 and 5. The near-wake recirculation region for Re=10,000 shrinks considerably for the roughened sphere case in Figs 4 and 5. The width of the shear layer after separation is small and increases due to the roll-up of the eddies. Turbulence structure after separation in the shear layer is weak with the fluctuations primarily in streamwise direction. After roll-

up and breakdown of vortex rings, the turbulence becomes three-dimensional and attains till nearly free stagnation point i.e., saddle point. Increasing the occurrence of the turbulence owing to the roughened surface leads to later flow separation of the boundary layer which induces to increase mixing process in the shedding vortices and entrainment. This is the reason why also length of the recirculation zone decreases for the roughened sphere case.

The vorticity structure of the flow showed that the wake was much narrower at the higher Reynolds number. The transition to turbulence in the boundary layer substantially decreases the wake size. The reverse flow region in the wake is significantly reduced and the motion in that region also becomes weak owing to the roughness effects. The vortices produced from the flow separation around the periphery of the sphere have a tendency to move inwards because of the lower pressures prevailing within the wake. At Re=10,000 in bottom row of Fig. 3, the shear-layer instability occurs right behind the sphere in a form of vortex rings, and the flow becomes turbulent in the near wake. Therefore, at Re = 10,000, the size of the recirculation region is smaller and the wake recovers more quickly than at Re=5,000. At both Reynolds numbers, large-scale waviness of vortical structures is observed in the wake and the plane containing the large-scale waviness changes randomly as stated by Yun et al. [8]. This waviness is more pronounced at Re = 10,000 than at Re=5,000. The mechanism responsible for this large-scale waviness of vortical structures is shown to be closely associated with the temporal evolution of vortices generated by the shear-layer instability. The flow is three-dimensional, and shedding vortices convey fresh fluid into the wake flow region, magnifying the entrainment thus developing many eddies.

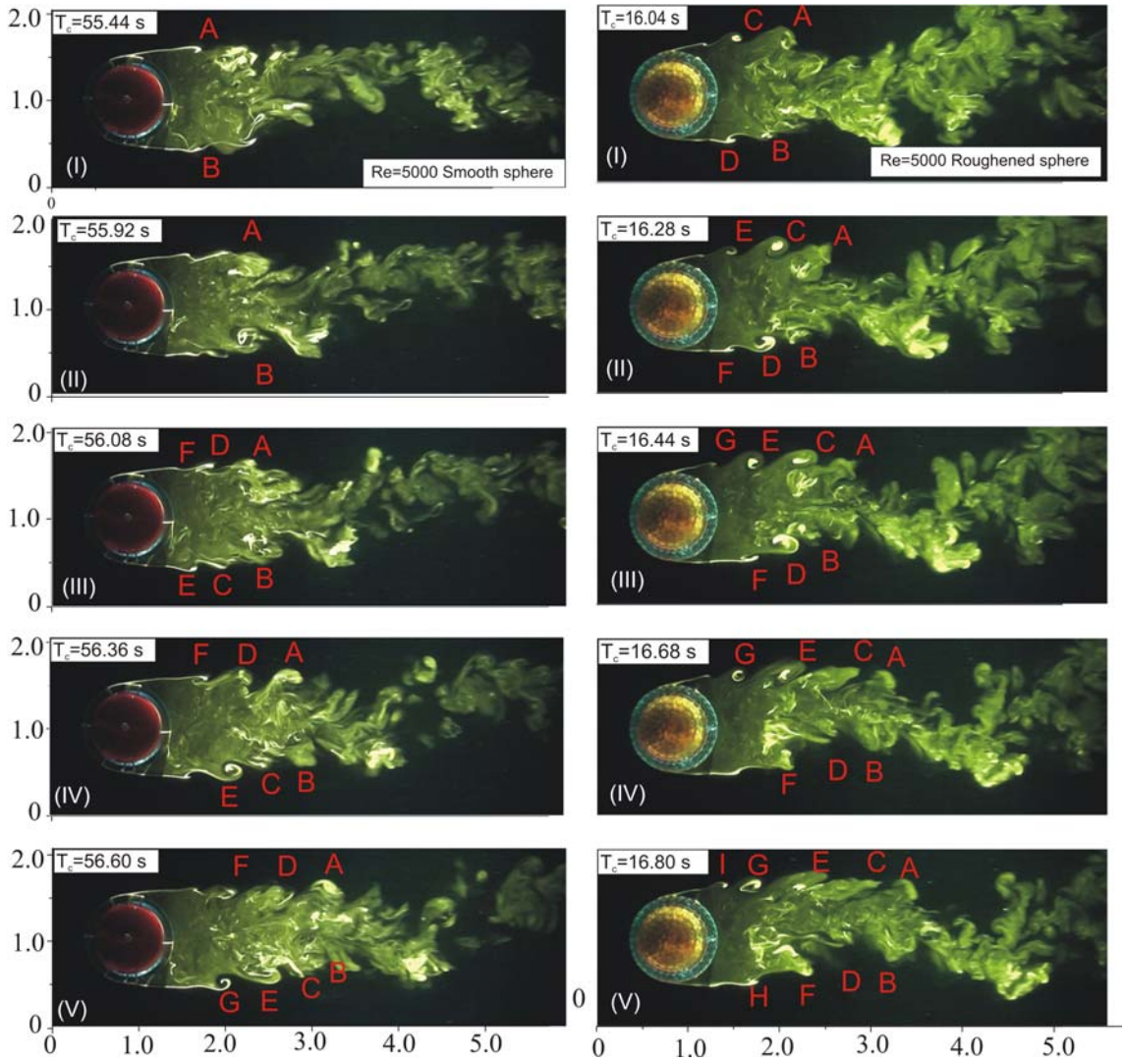

Figure 3: Comparison of flow visualization of flow structure with laser illumination of Rhodamine dye injection technique around the smooth sphere (left column) and the roughened sphere (right column) for Re=5000.

The instantaneous vorticity fields reveal an unsteady wavy structure of the sphere wake of Kelvin-Helmholtz structure as shown in Figure 3. The vortical flow structure in the near-wake region of the sphere shows an unsteady behavior and the onset of shear-layer instability. The appearance of the unsteadiness in the sphere wake could be the result of instability of the streamwise counter-rotating vortices. Comparison of time-averaged velocity fields $\langle V \rangle$, time-averaged streamline topology $\langle \Psi \rangle$ and streamwise velocity component contours $\langle u/U_\infty \rangle$ around the smooth sphere (left column) and roughened sphere (right column) for 5000≤Re≤10,000 are respectively shown in Figures 6, 7 and 8. A laminar boundary layer forms on the upstream surface of the sphere. The flow accelerates as it is deflected by the sphere and the deflected flow does not follow the sphere curvature so that the flow at around 90^o angle for the smooth sphere case separated and becomes turbulent in the wake. It is observed that the wake is unstable with vortex shedding. The mean velocity field showed two peculiar large-scale recirculation vortices downstream of the sphere model, and the length of the circulation region was approximately one diameter in the wake region for the smooth sphere. As seen in Fig 6, recirculation zone in the wake region of time-averaged velocity fields $\langle V \rangle$ for the roughened sphere case is weaker and shorter than that for the smooth sphere case.

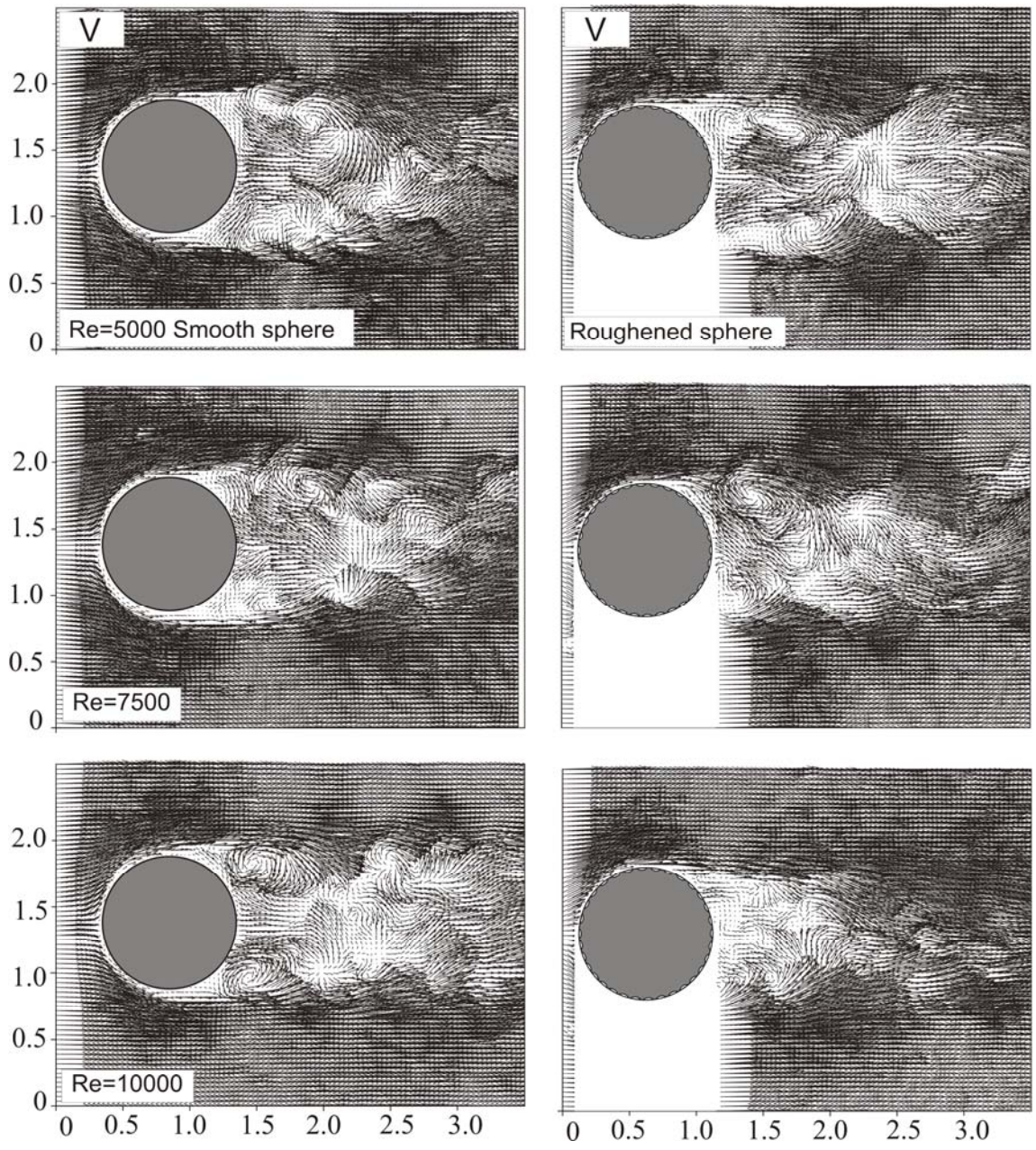

Figure 4: Comparison of instantaneous velocity fields V around the smooth sphere (left column) and roughened sphere (right column) for 5,000≤Re≤10,000.

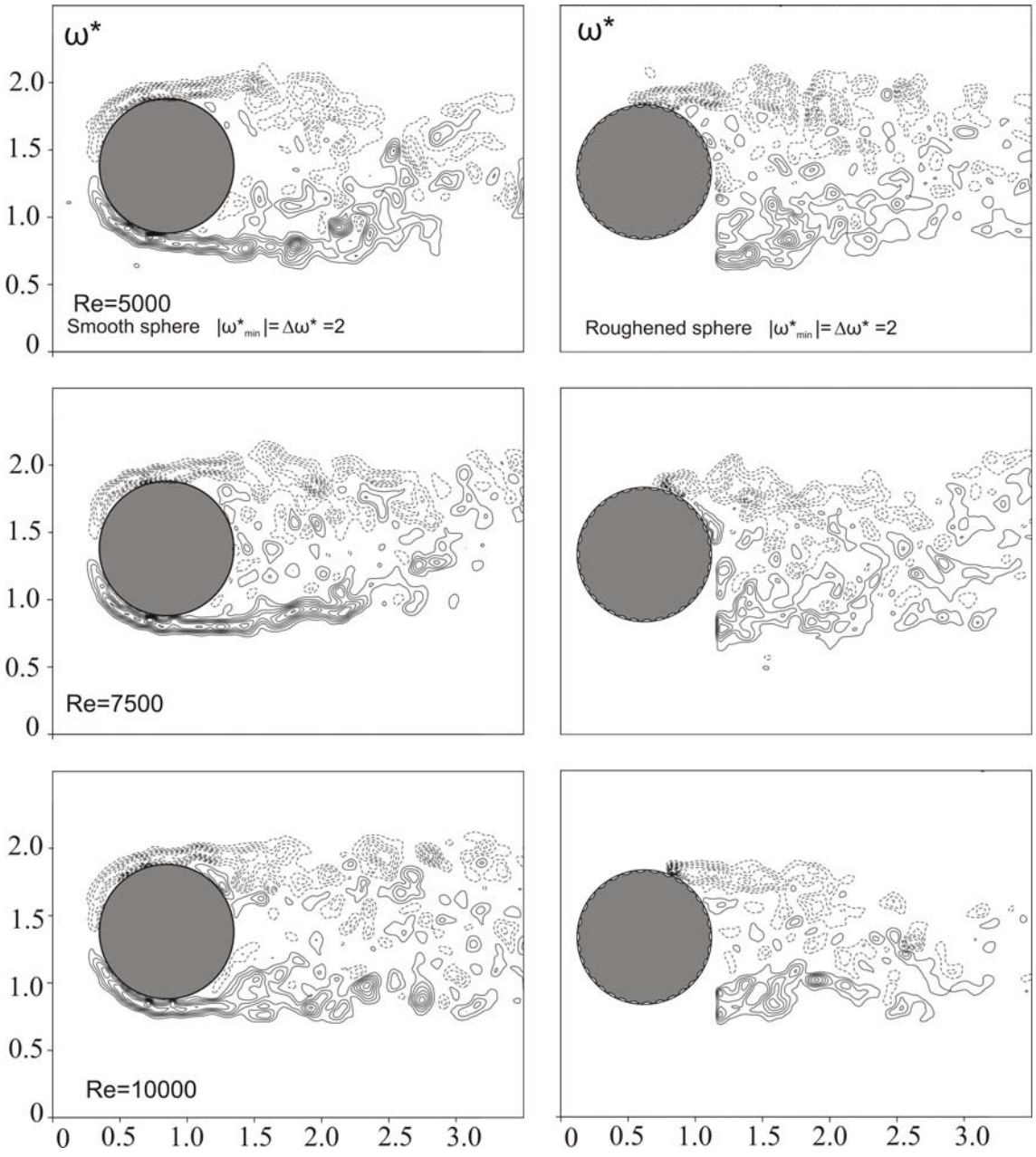

Figure 5: Comparison of instantaneous vorticity contours ω^* around the smooth sphere (left column) and roughened sphere (right column) for 2,500≤Re≤10,000.

As displayed in Fig 7, time-averaged streamline topology $\langle\Psi\rangle$ around the smooth sphere (left column) and roughened sphere (right column) for 5,000≤Re≤10,000 have two foci designated with F_1 and F_2 and one saddle point S. For all of the cases, the foci rotate inward direction which is evidence of stable flow patterns. However, instantaneous flow patterns exhibit completely unstable structure. The saddle point S locations from the smooth sphere base determined from time-averaged streamline patterns $\langle\Psi\rangle$ were found as 1.15, 0.99 and 0.88 for Re=5.000, 7,500 and Re=10,000, respectively. The transition from laminar to turbulence in the separated flow region occurs earlier as Reynolds number increases from Re=5,000 to 10,000. Moreover, in similar way, for the roughened sphere case in the left column of Fig 7, the saddle point S locations for time-averaged streamline patterns $\langle\Psi\rangle$ were occurred earlier as 1.13, 0.81 and 0.71 for Re=5.000, 7,500 and Re=10,000, respectively. Comparison of the time-averaged patterns shows that flow structures of the wake are almost equally symmetrical with respect to the centerline of the sphere without roughness whereas they are not symmetrical for the roughened sphere as well as the smooth sphere case owing to the specially hand-made roughness. The time-averaged streamline pattern shapes extended upstream to near base

region of the sphere with and without roughness are elliptical and have a limited spiral cycle that is lower for the roughened sphere case.

Streamwise velocity component contours $\langle u/U_\infty \rangle$ around the smooth sphere (left column) and roughened sphere (right column) for 5,000≤Re≤10,000 are presented in Fig 8. The minimum reverse velocity values U_{min} for Re=5.000, 7,500 and Re=10,000 were obtained as -0.451, -0.407 and -0.381, respectively, which decreases with increasing Reynolds number because of shrinking wake region. For the roughened sphere case, those peak values become significantly smaller for Re=7,500 and 10,000. Small circle in Fig 8 shows the positions of free stagnation point that those are respectively found to be 1.05D, 0.87D and 0.80D for Re=5,000, 7,500 and Re=10,000 for the smooth sphere case. They are shorter for the roughened sphere case and determined as 1.03D, 0.72D and 0.58D for Re=5,000, 7,500 and Re=10,000, respectively. The increment distance between contour levels around free stagnation point is larger than far wake region due to merging of separated flow around saddle point.

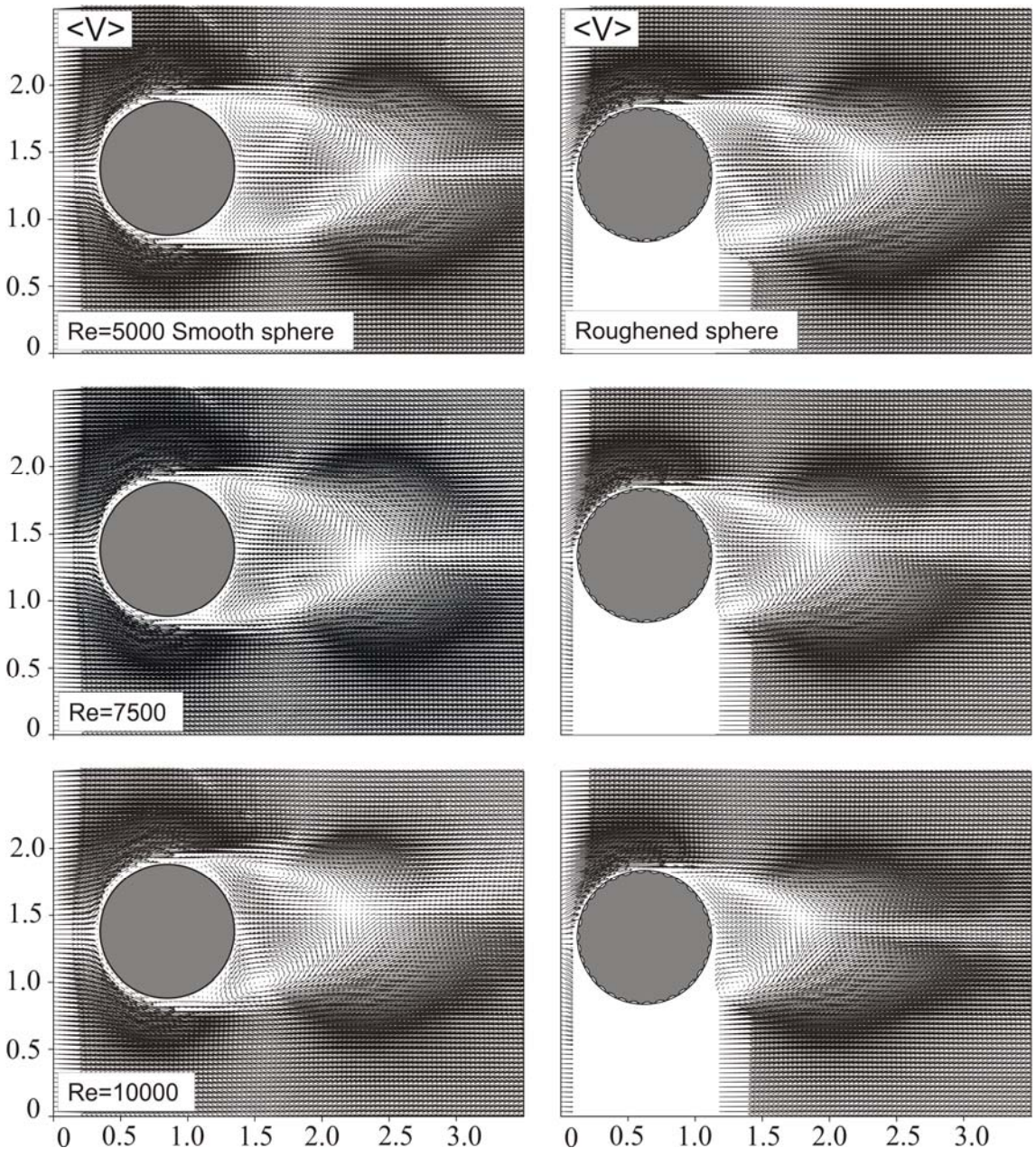

Figure 6: Comparison of time-averaged velocity fields $\langle V \rangle$ around the smooth sphere (left column) and roughened sphere (right column) for 5,000≤Re≤10,000.

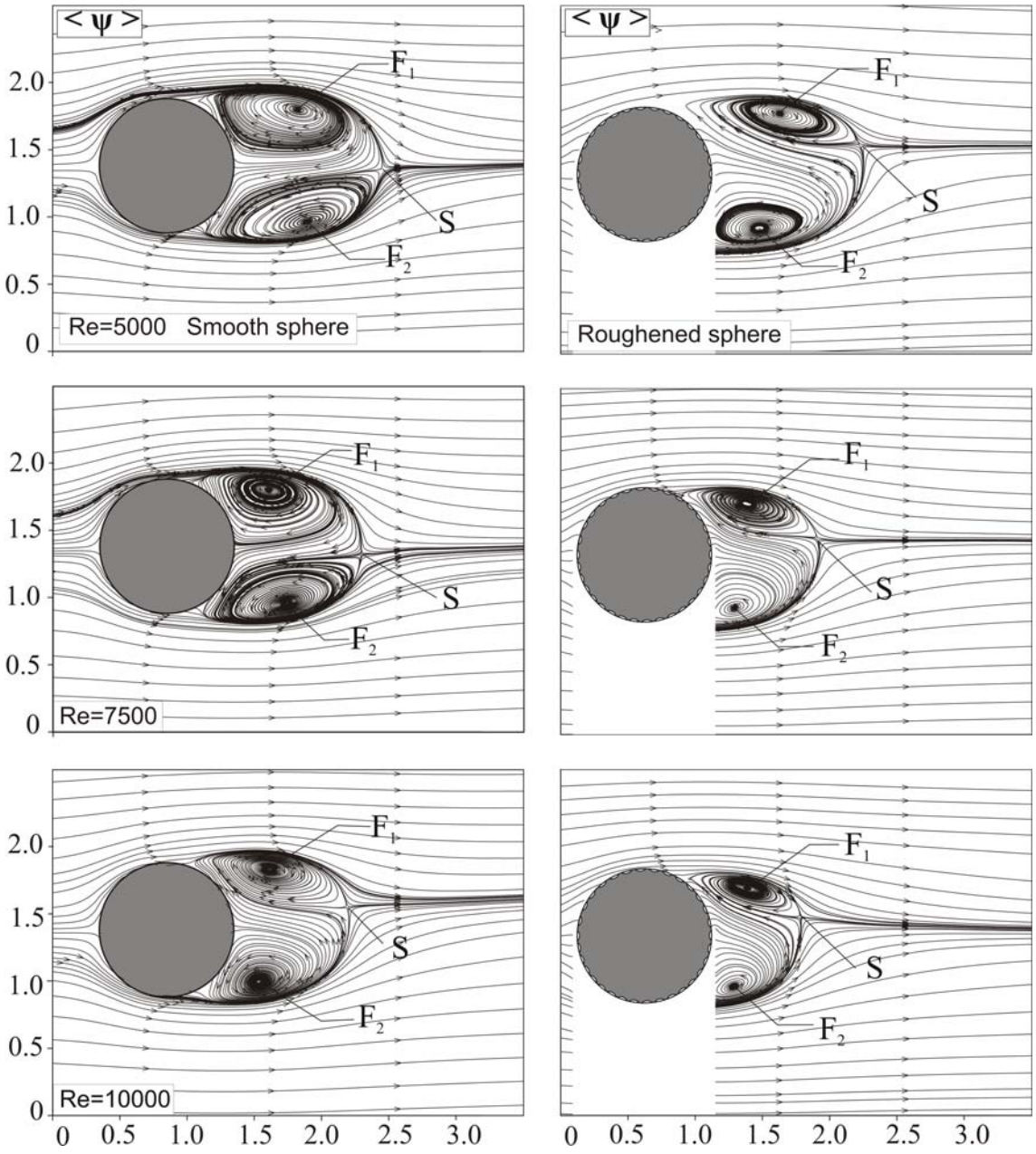

Figure 7: Comparison of time-averaged streamline topology <Ψ> around the smooth sphere (left column) and roughened sphere (right column) for 5,000≤Re≤10,000.

Comparisons of streamwise velocity fluctuations $<u_{rms}/U_\infty>$ and cross-stream velocity fluctuations $<v_{rms}/U_\infty>$ around the smooth sphere (top row) and roughened sphere (right column) for 5000≤Re≤10,000 are respectively presented in Figs 9 and 10. The streamwise velocity fluctuations $<u_{rms}/U_\infty>$ are the largest with maximum values in the shear layer. The rms streamwise velocity patterns $<u_{rms}/U_\infty>$ have detectable double peaks at almost equal distances in the upper and lower wake regions of the centerline for the smooth sphere and sphere with roughness while a single peak is seen in $<v_{rms}/U_\infty>$ with the maximum occurrence around the symmetry axis for all spheres. Their locations and magnitudes are given in Figs 9 and 10 for validation and comparison purposes. The maximum points of $<u_{rms}/U_\infty>$ and $<v_{rms}/U_\infty>$ become closer to the sphere base for the roughened sphere case. The shortest distance between sphere base and the maximum point of $<u_{rms}/U_\infty>$ and $<v_{rms}/U_\infty>$ occurs for Re=10,000 for both of the sphere cases. It can be explained that more momentum transfer occurs through the wake region due to the retarded flow separation. Therefore, it can be stated that the drag coefficient for the sphere with the roughness can specially decrease. Transverse velocity fluctuations $<v_{rms}/U_\infty>$ along the symmetry axis have a strong effect on the vortex

shedding. They increase rapidly until the peak points displayed in Fig 10 and decrease slightly to reach to free-stream flow condition. The value of cross-stream velocity fluctuations $\langle v_{rms}/U_\infty \rangle$ in axial direction increases slowly in the shear layer and takes the maximum at the end of the recirculation zone. Maximum value of the cross-stream velocity fluctuations $\langle v_{rms}/U_\infty \rangle$ for Re=7,500 happens for the smooth sphere case as shown in Fig 10.

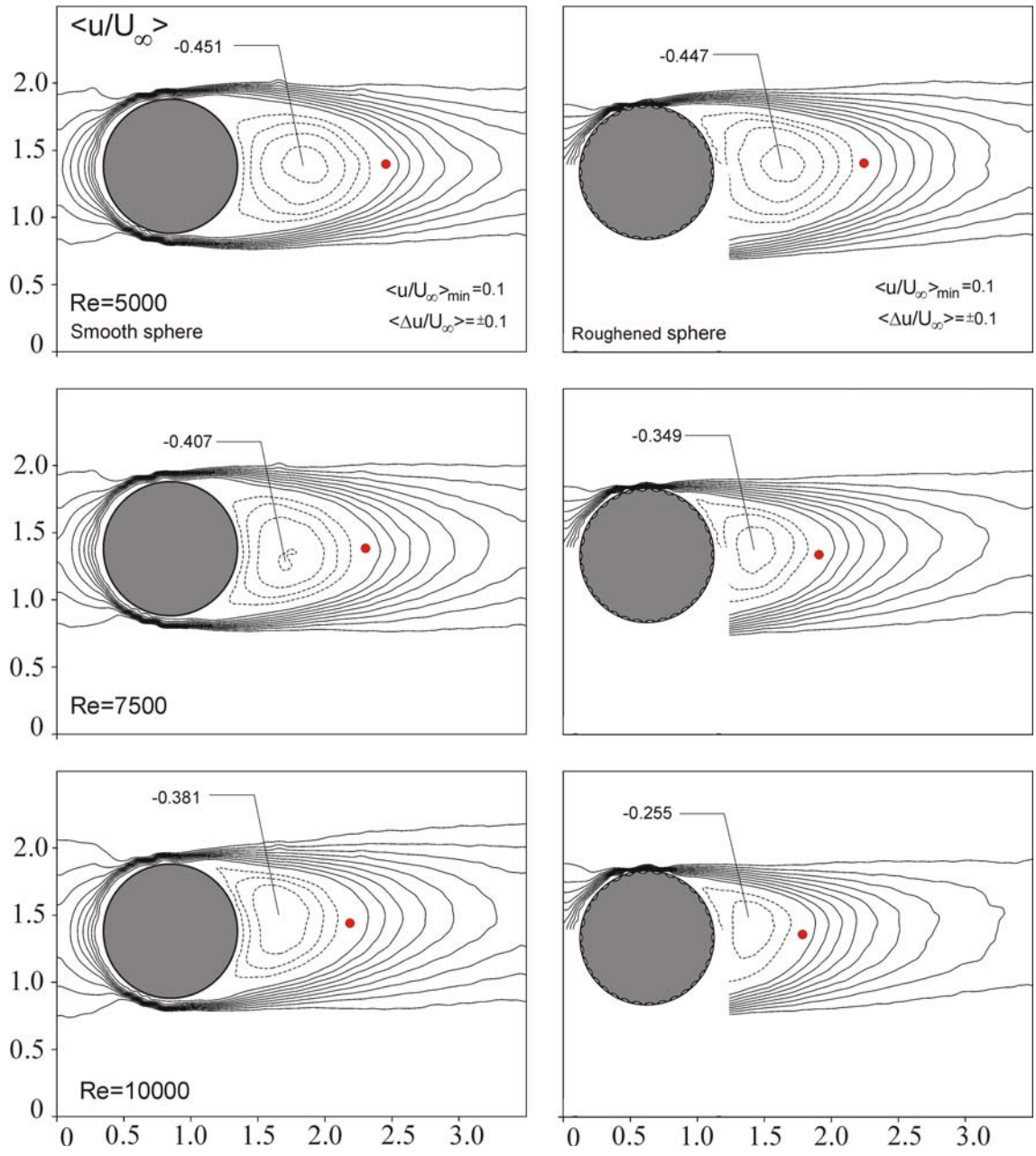

Figure 8: Comparison of streamwise velocity component contours $\langle u/U_\infty \rangle$ around the smooth sphere (left column) and roughened sphere (right column) for 5,000≤Re≤10,000.

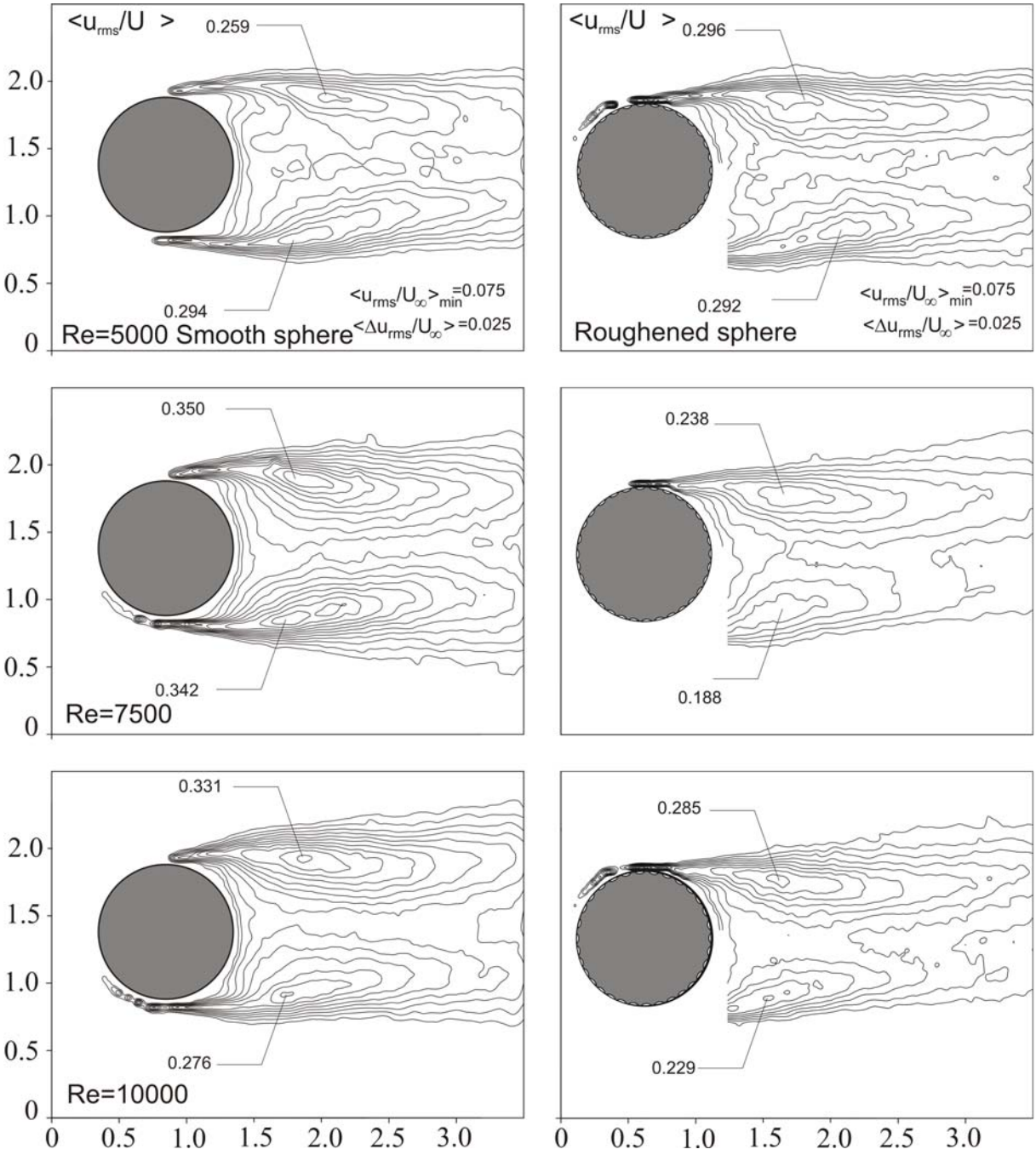

Figure 9: Comparison of streamwise velocity fluctuations $<u_{rms}/U_\infty>$ around the smooth sphere (top row) and roughened sphere (right column) for 5000≤Re≤10,000.

Comparison of Reynolds stress correlations $< u'v'/U_\infty^2 >$ around the smooth sphere (left column) and roughened sphere (right column) for 5000≤Re≤10,000 is given in Fig 11. Reynolds stress correlations $< u'v'/U_\infty^2 >$ do not have contours close around the sphere and they have the larger values in the free shear layer. At a Reynolds number of Re = 10,000 for the roughened sphere, the boundary layer switches from being predominantly laminar to predominantly turbulent, hence the separation point moves further downstream and the wake narrows. Well-defined Reynolds stress patterns due to fluctuations along the shear layers. This behavior of the flow provides the momentum transfer from the free-stream flow into the wake region due to pressure difference between the wake and free-stream flow. The upstream extension of each large-scale clusters occurs further upstream, and the tip of the large-scale clusters is located closer to the base of the sphere for all Reynolds numbers as shown in Fig. 11. Magnitudes of the Reynolds stress correlations are not so different that the surface modifications as examined in the present study may not always effectively in all cases because there could be a need to retain the structural geometry due to design considerations as well as application

of Reynolds number range. The patterns of the Reynolds stress correlations consist of two large-scale clusters located just downstream. Another important point is that the peak concentrations of Reynolds stress occurred very close to the saddle points for both the smooth and roughened sphere cases. Peak values of the positive Reynolds stress correlations decrease for the roughened sphere case due to the retarded separation point .

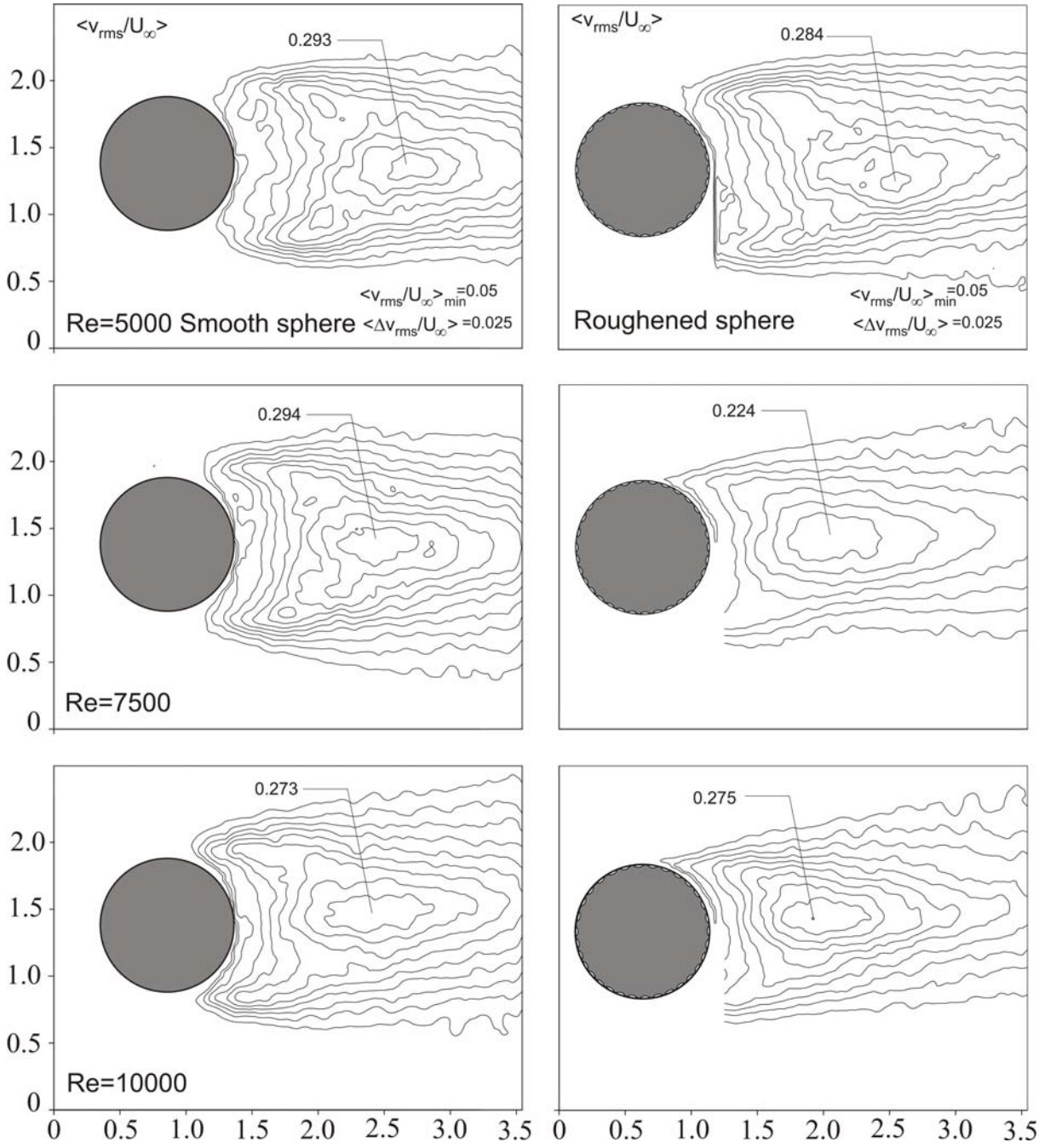

Figure 10: Comparison of cross-stream velocity fluctuations $\langle v_{rms}/U_\infty \rangle$ around the smooth sphere (left column) and roughened sphere (right column) for 5,000≤Re≤10,000.

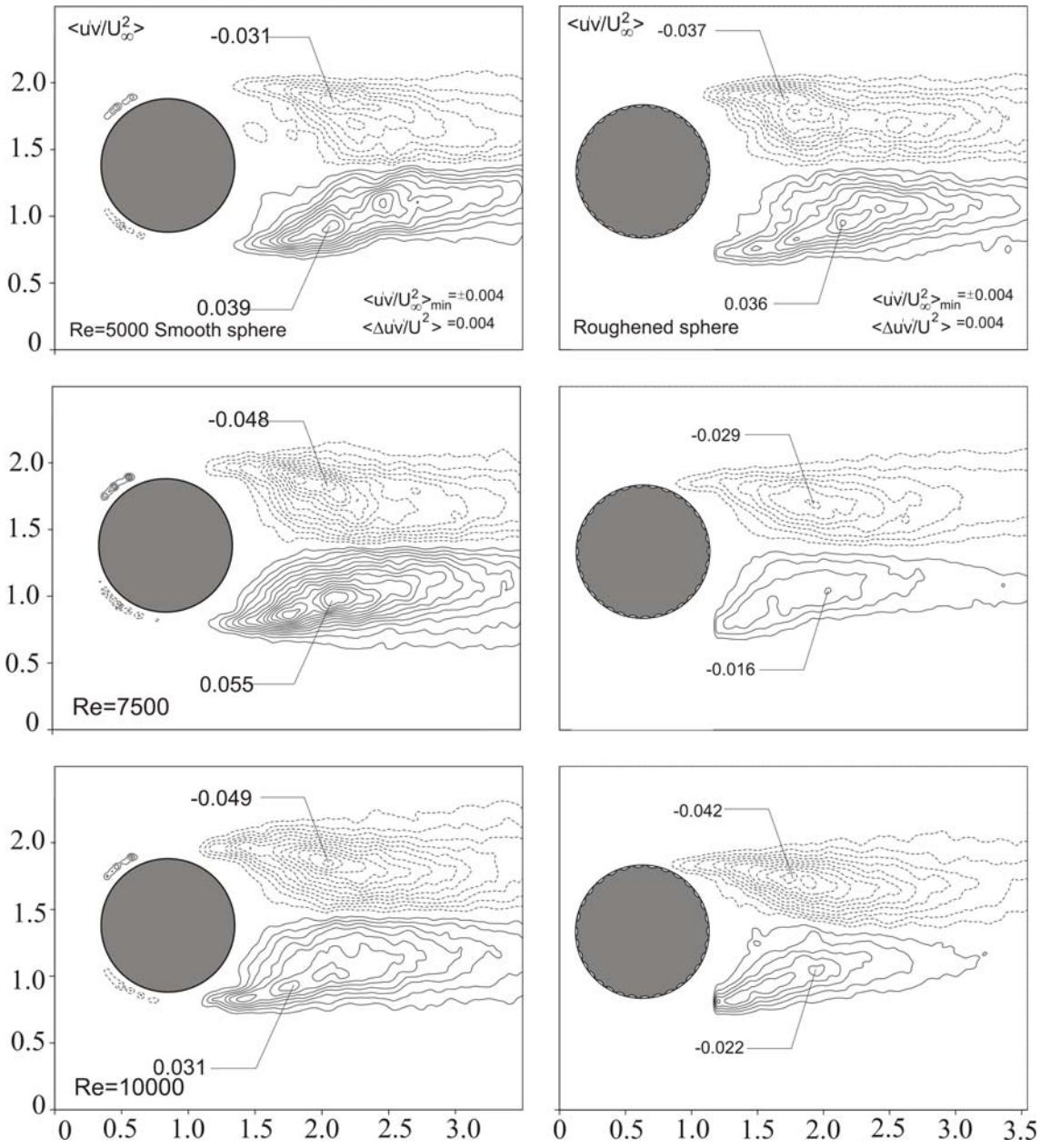

Figure 11: Comparison of Reynolds stress correlations $< u'v'/U_\infty^2 >$ around the smooth sphere (left column) and roughened sphere (right column) for 5000≤Re≤10,000.

CONCLUSIONS

The obtained results for the roughened sphere were compared with the corresponding results from a smooth sphere and the following findings were derived.

It is observed from dye visualization that high frequency periodicity characteristic of Kelvin-Helmholtz instability in the separating laminar shear layer is also evident from undulations in the interfacial layer between the wake and free-stream for both the smooth and the roughened sphere cases. The flow is three-dimensional, and shedding vortices convey fresh fluid into the wake flow region, magnifying the entrainment thus developing many eddies. The near-wake recirculation region shrinks considerably while a complex evolution of vortex structures in the near wake maintains. The small-scale Kelvin-Helmholtz instability leads to rapid transition of the separated shear layer, with consequent irregular perturbation of the interfacial layer that leads to entrainment of process and contributes to the decrement in wake size for the roughened sphere. For 5000≤Re ≤10000, the flow in the wake becomes turbulent while the flow in the boundary layer remains laminar, i.e. turbulent flow with laminar boundary layers. A laminar flow separation for the smooth sphere was found to occur

near the equator while that for the roughened sphere was retarded. The smooth laminar shear layers appeared to be axisymmetrically. For the case of the roughened sphere, at a Reynolds number of Re=10000, the boundary layer occurs predominantly turbulent, hence the separation point moves further downstream. The vorticity structure of the flow showed that the wake was much narrower for the roughened sphere. At Re=10,000 the flow in the wake becomes turbulent while the flow in the boundary layer remains laminar. The roughness causes local flow separation and trigger the shear layer instability along the separating shear layer, resulting in the attenuation of large magnitude of flow intensity characteristics. The reverse flow region in the wake is significantly reduced and the motion in that region also becomes weak owing to the roughened sphere surface. The PIV measurements in the streamwise plane for 5,000≤Re ≤10,000 clearly revealed the turbulent structures of the sphere wake such as recirculating flow, shear layer instability, vortex roll-up, and small-scale turbulent eddies. The saddle point locations from the sphere base in the wake region for time-averaged streamline patterns were determined for the smooth/ the roughened sphere as 1.15/1.13 at Re=5000, 0.99/0.81 at Re=7500 and 0.88/0.71 at Re=10,000, respectively. Moreover, the transition from laminar to turbulence in the separated flow region occurred earlier as Reynolds number increases from Re=5,000 to 10,000. However, the physical mechanisms associated with the frequencies other than the vortex shedding frequency are not clear at this point and are the subject of an ongoing study. Experimental data obtained here can serve the goal of validation of turbulence models used in numerical simulations and in predicting bluff body flows in the sub-critical regime.

ACKNOWLEDGMENT

The authors would like to acknowledge the funding of the Scientific and Technological Research Council of Turkey (TÜBİTAK) under contract No:109R028, Coordinatorship of Selcuk University's Scientific Research Project and Scientific Research Projects Office of Cukurova University under contract No: AAP20025.

References

[1] Son, K., Choi, J., Jeon, W.P. and Choi, H., *Mechanism of drag reduction by a surface trip wire on a sphere*, J. of Fluid Mechanics, 672, p:411-427, 2011.

[2] Ozgoren, M., Okbaz, A., Kahraman, A., Hassanzadeh, R., Sahin, B., Akıllı, H. and Dogan, S., *Experimental Investigation of the Flow Structure around a Sphere and Its Control with Jet Flow via PIV*, The sixth International Advanced Technologies Symposium 16-18 May 2011, Fırat University, Elazıg, Turkey, accepted for presentation, 2011.

[3] Ozgoren, M., Dogan, S., Okbaz, A., Kahraman, A., Hassanzadeh, R., Sahin, B. and Akıllı, H., *Passive Control of Vortical Flow Structure around a Sphere by an O-ring*, The sixth International Advanced Technologies Symposium 16-18 May 2011, Fırat University, Elazıg, Turkey, The sixth International Advanced Technologies Symposium 16-18 May 2011, Fırat University, Elazıg, Turkey, accepted for presentation, 2011.

[4] Ozgoren, M., Şahin, B., Pınar, E., ve Akıllı, H., *Experimental Investigation of Flow structure around a Sphere and Cylinder via Flow Visualization*, 5. Ankara International Aerospace Conference, AIAC-2009-012, 17-19 August, 2009. - METU, Ankara.

[5] Kumar, R.A., Sohn, C.H. and Gowda, B.H.L., *Passive Control of Vortex-Induced Vibrations: An Overview*, Recent Patents on Mechanical Engineering, 1, 1-11, 2008.

[6] Young II, J., and Lee, S.J., *PIV analysis of near-wake behind a sphere at a subcritical Reynolds number, Experiments in Fluids*, Vol. 44, Issue 6, p:905-914, 2008.

[7] Ozgoren, M., Şahin, B., Akıllı, H., Karakuş, C., Yayla, S., Öztürk, A. ve Akar, A., *Küre Etrafındaki Akış Yapısının Parçacık Görüntülemeli Hız Ölçme Yöntemiyle İncelenmesi*, UHUK 06-028, ODTÜ Ankara, 21-23 Eylül 2006.

[8] Yun, G., Kim, D. and Choi, H., *Vortical structures behind a sphere at subcritical Reynolds numbers*, Phys. Fluids 18, 015102 ,2006.

[9] Choi, J., Jeon, W. and Choi, H., *Mechanism of drag reduction by dimples on a sphere*, Physics of Fluids, 18, 041702, 2006.

[10] Jeon, S., Choi, J., Jeon,W., Choi, H. and Park, J., *Active control of flow over a sphere for drag reduction at a subcritical Reynolds number*, J. Fluid mech. vol. 517, p:113–129, 2004.

[11] Alammar, K.N., *Turbulent flow over a sphere with suction and blowing holes and a golf ball: a numerical study*, 22nd Applied Aerodynamics Conference and Exhibit, Providence, Rhode Island, 16 - 19 Aug 2004.

[12] Vukman, B., *Experimental investigation of a flow around a sphere,* Thermal Science, Vol.8 No.1, p:63 – 81, 2004.
[13] Kiya, M., Ishikawa, H., Sakamoto, H., *Near-wake instabilities and vortex structures of three-dimensional bluff bodies*: a review, J. Wind Eng Ind Aerodyn, Vol. 89, p:1219–1232, 2001.
[14] Suryanarayana, G.K., Prabhu, A., *Effect of natural ventilation on the boundary layer separation and near-wake vortex shedding characteristics of a sphere*, Exp. Fluids 29, Issue 7, p:582–591, 2000.
[15] Hart, D.P., *PIV error correction*, Exp. Fluids 29, p:13–22, 2000.
[16] Fouras, A., Soria, J*., Accuracy of out-of-plane vorticity measurements derived from inplane velocity field data,* Exp. Fluids, Vol.25, 409–30, 1998.
[17] Gad-el-hak, M., *Modern developments in flow control*, Applied Mechanics reviews, vol. 49, p:65–379, 1996.
[18] Suryanarayana, G.K., GEA, M., *Effect of ventilation on the flow field around a sphere*, Exp Fluids 19, p:78-88, 1995.
[19] Bearman, P.W. and J. Harvey, K., *Control of circular cylinder flow by the use of dimples*, AIAA J. 31, p:1753-1756,1993.
[20] Westerweel, J., *Digital particle image velocimetry, theory and application*, Delft University Press, 1993.
[21] Adrian, R.J., *Particle-imaging techniques for experimental fluid mechanics*, Annu. Rev.Fluid Mech., Vol.23, 261–304, 1991.
[22] Sakamoto, H., Haniu, H., *A study on vortex shedding from spheres in a uniform flow*, J. Fluids Eng Vol.112, p:386–392, 1990.
[23] Keane, R.D., Adrian R.J., *Optimization of particle image velocimeters*, Opt. Methods Flow Particle Diagnostics. 68, p:139–159, 1989.
[24] Kim, H. J. & Durbin, P. A., *Observations of the frequencies in a sphere wake and of drag increase by acoustic excitation*, Phys. Fluids 31, p:3260–3265, 1988.
[25] Nakamura, Y., and Tomonari, Y., *The effects of surface roughness on the flow past circular cylinders at high Reynolds numbers*, J. Fluid Mech. 123, p:363, 1982.
[26] Werle, H., *ONERA photograph In: An album of fluid motion (assembled by Dyke V)*, Parabolic Press, Stanford, pp 32–35, 1980.
[27] Taneda, S., *Visual observations of the flow past a sphere at Reynolds numbers between 10^4 and 10^6*, J. Fluid Mech., 85, p.187-192, 1978.
[28] Bearman, P.W. and Harvey, J.K., *Golf ball aerodynamics Aeronaut*. Q. 27, 112,1976.
[29] Winant, C.D., Browand, F.K., *Vortex pairing, the mechanism of turbulent mixing-layer growth at moderate Reynolds numbers*, J. Fluid Mechanics, Vol.63, p:237-255, 1974.
[30] Achenbach, E*., Vortex shedding from spheres*, J.Fluid Mech 62(2), p.209–221, 1974.
[31] Achenbach, E., *Experiments on the flow past spheres at very high Reynolds numbers*, J. Fluid Mech 54(3), p:565–575, 1972.
[32] Maxworthy, T., *Experiments on the flow around a sphere at high Reynolds numbers*, J. Appl. Mech. 36, p:598, 1969.